Proceedings of the Sixth International Conference on
Railway Technology: Research, Development and Maintenance
Edited by: J. Pombo
Civil-Comp Conferences, Volume 7, Paper 24.1
Civil-Comp Press, Edinburgh, United Kingdom, 2024
ISSN: 2753-3239, doi: 10.4203/ccc.7.24.1

Non-Uniform Expansion Characteristics of Red Beds in the Sichuan Basin, China: Implications for Uplift Mechanisms in High-Speed Railway Subgrade

F. Yu, J. Li, Z. Dai and S. Chen

**State Key Laboratory of Geomechanics and Geotechnical Engineering,
Institute of Rock and Soil Mechanics, Chinese Academy of Sciences
Wuhan, China**

Abstract

The sustained uplift deformation issue in high-speed railway subgrades in the Sichuan Red Beds region poses a long-term and potential threat to operational safety. Through reliance on practical engineering, this study conducts micro-fine-scale testing, triaxial expansion characteristic experiments, and in-situ layered uplift monitoring in the Sichuan Red Beds region. It analyzes the non-uniform expansion characteristics caused by differences in mineral composition, microstructural organization, and rock layer structure at different scales. The study explores the mechanism of its long-term uplift effect on the subgrade. The results indicate significant variations in the types and content of expansive clay minerals produced in the interlayers of the Sichuan Red Beds. Coupled with the preferential orientation of microscopic particles, this leads to high expansion force, a wide range of values, and noticeable anisotropy. This non-uniform expansion deformation creates macro-micro cracks, influencing the measured layered uplift quantity controlled by joint and fracture surface distribution. It is also identified as a crucial mechanism for the sustained non-convergent uplift deformation of the subgrade under the influence of repeated environmental changes. The research findings provide practical reference for high-speed railway construction and disease treatment in the Sichuan region.

Keywords: Red Beds, moisture absorption expansion, non-uniformity, fracture, uplift, high-speed railway subgrade.

1 Introduction

The Red Beds, deposited in high-temperature and oxidizing environments, constitute a set of red continental strata widely distributed in China, with the most concentrated presence in the southwestern region, accounting for approximately 33% of the total national red bed area. Among these, the Sichuan Basin stands out as the most typical region for red beds. Often referred to as the “Red Basin”, the extensive distribution of red beds in the Sichuan Basin primarily formed during the Jurassic and Cretaceous periods [1]. Comprising alternations of soft and hard mudstone and breccia, these deposits originated from the river-lake depositional environment of the ancient Ba-Shu Lake Basin. The mudstone in these formations generally contains a significant amount of hydrophilic clay minerals, leading to characteristics such as expansion, disintegration, and softening. These features make the red beds highly susceptible to engineering issues such as uplift in subgrades and slope instability. The susceptibility to expansion, disintegration, and softening poses challenges [2-6] and can trigger various engineering problems, including uplift in subgrades and slope instability.

With the construction and operation of the high-speed railway network in the distribution area of the red beds in the Sichuan Basin, the issue of uplift diseases in high-speed railway subgrades, where deformation control is extremely stringent, has attracted widespread attention[7]. Researchers have conducted relevant studies on the causative mechanisms of this problem. Yu et al. [8] conducted a study on the micro-fine-scale expansion mechanism of red bed mudstone in the Sichuan Basin. Feng et al. [9] carried out in-situ expansion deformation tests and laboratory pressure water expansion deformation tests on weakly weathered mudstone. Huang et al. [10] investigated the influence of pH value on the moisture absorption expansion of red bed mudstone and its microscopic mechanism. Wu et al. [11], combining laboratory expansion tests, used the CVISC viscoelastic-plastic model in FLAC3D to simulate the vertical deformation generated during trench excavation. Ji et al. [12], starting from the perspective of rheology of red bed soft rock, analyzed the uplift deformation pattern of deep excavation trench bases using elastic-plastic and viscoelastic-plastic models in FLAC3D software. Zhang et al. [13] conducted large-scale expansive tests on the mudstone foundation of the Lanxin high-speed railway. Wang et al. [14] elaborated on the development laws of one-way and multi-directional expansion deformations under water immersion conditions in high-speed railway mudstone foundations. Dai et al. [15], combining field monitoring data, explored the causes of long-term uplift in the Chengyu high-speed railway subgrade. Chen et al. [16] observed the evolution characteristics of cracks during the water immersion process of mudstone in the Sichuan Basin. Jing [17] studied the hydraulic characteristics of the red beds in the Sichuan Basin and the mechanism of their impact on the deformation of ballastless track.

The majority of the aforementioned studies have treated the mudstone in the red beds of the Sichuan Basin as a uniformly homogeneous unit to analyze and investigate its disaster-causing mechanisms. However, in reality, the red beds in the Sichuan Basin exhibit significant non-uniformity in both macroscopic stratigraphic structure

and mineral composition, as well as microscopic organization. The resulting non-uniform expansion deformation is an essential mechanism leading to the formation and expansion of fractures in the mudstone of the red beds [18-19]. To further deepen our understanding of this mechanism, based on practical engineering, we conducted micro-fine-scale testing, triaxial expansion rate experiments, and on-site layered uplift deformation monitoring in the Sichuan red beds. By examining the material composition and the non-uniform characteristics of the structure at different scales, as well as the anisotropic features of expansion indicators in the red beds, we aim to analyze their correlation with the spatiotemporal evolution of actual stratigraphic uplift deformation. This research seeks to investigate the significant role played by the non-uniform expansion deformation of the red beds in the Sichuan Basin during the long-term uplift process in subgrades.

2 Non-uniform Characteristics of the Red Beds

Fig. 1 depicts the typical stratigraphic structure of the red beds in the Sichuan Basin, comprising interbedded layers of mudstone, silty sandstone, and sandstone, forming nearly horizontal layers. Cementing materials include clay, calcium, and iron, contributing to an incomplete formation. Joints and fractures are prevalent, with uneven distribution of orientations within the rock mass. Mudstone exhibits poor resistance to weathering and low strength, while sandstone is stable and possesses higher strength, resulting in distinct weathering characteristics. This alternation of soft and hard layers is common in the red beds. Mudstone's poor permeability acts as an impermeable layer, contrasting with sandstone's good permeability, creating a hydraulic connection channel. This leads to liquefaction of mudstone at the interlayer interface, forming a weak layer prone to displacement under tectonic stress and engineering disturbances.

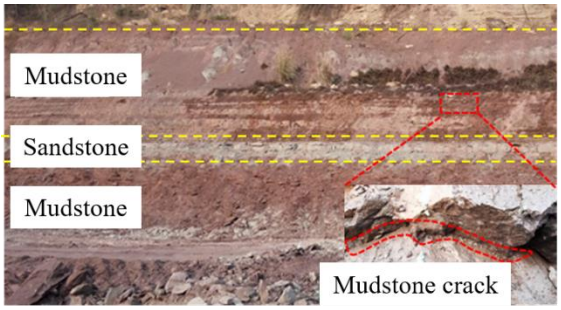

Figure 1: Typical rock structure of red-bed in Central Sichuan.

Predominant detrital minerals include quartz and feldspar, with mudstone containing significant clay minerals such as montmorillonite, illite, and chlorite, establishing the expansive nature of mudstone. Moisture absorption tests reveal uneven swelling due to non-uniform distribution of clay minerals, possibly influenced by particle size, distribution, and mineral composition during sedimentation.

Fig. 2 presents SEM images, showing curled and sheet-like clay minerals primarily in mudstone, along with honeycomb-like aggregation and slender micro-cracks.

Sandstone exhibits feldspar and quartz aggregates with oriented long axes and fewer micro-cracks, indicative of a dense structure.

In summary, the non-uniform characteristics of the microscopic structure in the red beds of the Sichuan Basin are mainly manifested by the presence of curled clay minerals filling the pores and fractures between platy detrital particles, forming a surrounding-type stacking arrangement in the form of interlayers. The oriented arrangement of mineral particles, especially the preferential orientation of clay mineral plate aggregates, is a microscopic mechanism leading to the anisotropy of the physical and mechanical properties in the red beds of the Sichuan Basin.

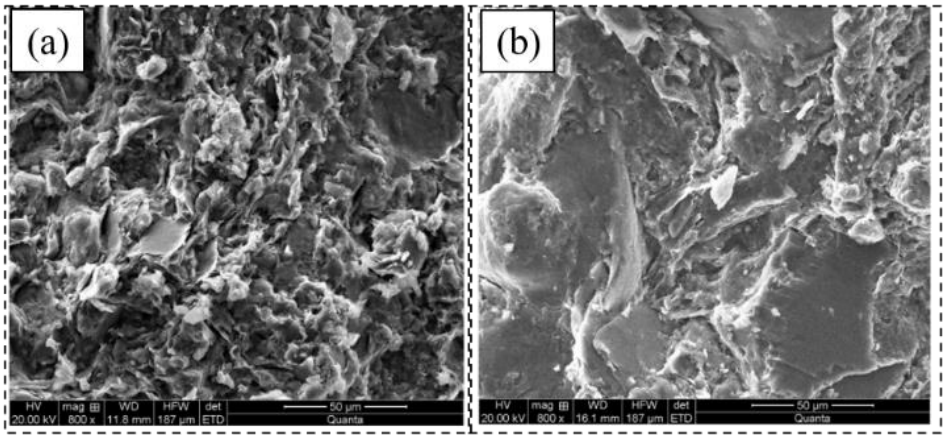

Figure 2: Electron microscopic scanning of the red beds in Central Sichuan: (a) Mudstone, (b) Sandstone.

3 Non-uniform Expansion Characteristics

In order to understand the expansion characteristics of the red beds in the Sichuan Basin, expansion rate tests and expansion force tests were conducted using original rock samples. Table 1 presents the results of the triaxial expansion rate tests, where ε_x, ε_y, and ε_z represent the radial (X/Y directions) and axial (Z direction) expansion rates of the cylindrical specimens. It can be observed that the mudstone exhibits significant expansivity, with the primary expansion occurring in the axial direction (ε_z) perpendicular to the bedding. The range of axial expansion rates (ε_z) for mudstone is between 2.73% and 5.83%. In comparison, the expansivity of sandy mudstone is relatively weaker, with axial expansion rates ranging from 1.52% to 1.78%. Sandstone, on the other hand, shows minimal expansion, with axial expansion rates only between 0.07% and 0.12%, indicating its lack of significant expansivity.

No.	Rock type	Triaxial expansion rate			$R_x=\varepsilon_x/\varepsilon_z$	$R_y=\varepsilon_y/\varepsilon_z$	$R_0=R_x+R_y/2$
		ε_x/%	ε_y/%	ε_z/%			
1	Mudstone	1.66	1.71	2.73	0.61	0.63	0.62
2	Mudstone	2.31	2.03	3.07	0.75	0.66	0.71
3	Mudstone	1.48	1.53	3.69	0.40	0.41	0.41
4	Mudstone	3.68	3.72	5.49	0.67	0.68	0.67
5	Mudstone	1.82	2.23	3.38	0.54	0.66	0.60
6	Mudstone	1.42	1.64	3.59	0.40	0.46	0.43
7	Mudstone	2.44	3.14	5.83	0.42	0.54	0.48
8	Mudstone	1.37	1.44	4.15	0.33	0.35	0.34
9	Sandy mudstone	0.67	0.53	1.52	0.44	0.35	0.39
10	Sandy mudstone	0.89	0.96	1.78	0.50	0.54	0.52
11	Sandstone	0.17	0.08	0.07	-	-	-
12	Sandstone	0.06	0.10	0.12	-	-	-

Table 1: The results of the triaxial expansion rate tests.

Fig. 3, taking the example of Sample 1#, illustrates the expansion deformation time-history curves in the three directions. It can be observed that the development process of expansion rates in all three directions is generally synchronous, undergoing three stages: rapid expansion, slow expansion, and asymptotic stability. Additionally, it is evident that the radial expansion rates (ε_x, ε_y) of mudstone are significantly lower than the axial expansion rate (ε_z). The radial expansion rates of mudstone, as listed in Table 2, fall within the range of 1.37% to 3.72%.

In order to facilitate a unified description of the relative relationships between expansion rates in different directions, the coefficients of anisotropic expansion rates are defined as follows:

$$\mathrm{R_x} = \varepsilon_x/\varepsilon_z \quad (1)$$

$$\mathrm{R_y} = \varepsilon_y/\varepsilon_z \quad (2)$$

$$\mathrm{R_0} = (\mathrm{R_x} + \mathrm{R_y})/2 \quad (3)$$

In the formula, $\mathrm{R_x}$ and $\mathrm{R_y}$ represent the ratios of radial expansion rates in the X and Y directions to the axial expansion rate in the Z direction, respectively. $\mathrm{R_0}$ is the mean of $\mathrm{R_x}$ and Ry, which comprehensively reflects the ratio of expansion rates parallel to the bedding direction to the expansion rate perpendicular to the bedding direction. A smaller value of $\mathrm{R_0}$ indicates a more significant anisotropy in the expansion rates.

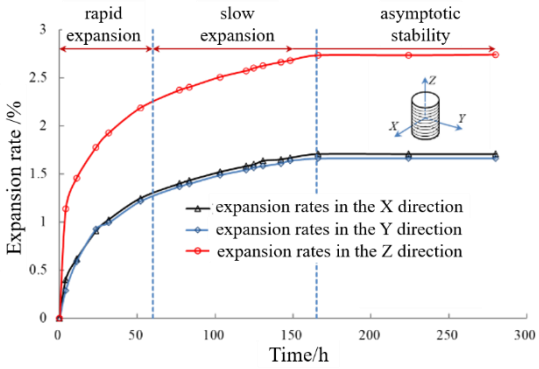

Figure 3: Time-history curve of swelling ratio.

In Table 1, the values of R_x, R_y, and R_0 for the red beds in the Sichuan Basin are also listed. It can be observed that the difference between R_x and R_y is relatively small, indicating a minor anisotropy in the direction parallel to the bedding. The range of the average value R_0, which reflects the anisotropy between the directions parallel and perpendicular to the bedding, is between 0.34 and 0.71. This suggests that the expansion rate parallel to the bedding is significantly smaller than the expansion rate perpendicular to the bedding. The mudstone in the red beds of the Sichuan Basin exhibits pronounced anisotropic expansivity, which is correlated with the preferential orientation of clay minerals in its microscopic structure.

The expansion force of mudstone is very high, ranging from 449.9kPa to 2025.5kPa. Despite the relatively moderate expansion rates of mudstone (2.73% to 5.83%), the generated expansion force under constrained expansion deformation is substantial. This poses a significant threat to the stability of engineering structures.

Integrating the experimental results of the expansion characteristics, it is evident that mudstone exhibits a wide range of expansion rates and expansion force values. The significant variability in the coefficients of anisotropic expansion rates also indicates that the expansion deformation of mudstone in the red beds of the Sichuan Basin is highly uneven. This uneven expansion, determined by the non-uniformity in mineral composition and microscopic structure, generates elevated internal stresses. For instance, the stress difference between the minimum expansion force of 449.9 kPa and the maximum expansion force of 2025.5 kPa is 1575.6 kPa. Such a high differential stress is sufficient to disrupt the internal structure of mudstone, leading to the generation and propagation of new fractures.

On the other hand, considering the composition and structure of the red beds in the Sichuan Basin, the interbedded structure of mudstone and sandstone exhibits significant differences in expansion rates and expansion forces. Uneven expansion, especially when exposed to water, can easily lead to interlayer slippage and cracking, providing new pathways for moisture migration. This, in turn, further triggers expansive deformation in the deeper rock mass.

4 The evolution patterns of in-situ expansion deformation

Since its opening in 2015, a section of the high-speed railway embankment in the red beds of the Sichuan Basin has experienced sustained uplift for several years. To understand the development trend of uplift deformation in this embankment, deformation monitoring points were set up on the embankment surface in June 2015. Static leveling sensors were installed on the track baseplate for monitoring. Figure 4 illustrates the layout of 22 measurement points along Mainline I. Points 1 to 13 are located in the arched section from station K152+670 to K152+911, while points 14 to 22 are in the arched section from station K153+595 to K153+770. The spacing between measurement points is 20 meters.

In December 2017, additional layered uplift deformation monitoring was implemented at points with significant uplift deformation. Multiple single-point settlement instruments were used to create monitoring arrays, placed between Mainline I and Line 3 and on the outer side of Line 3, as shown in Figure 4.

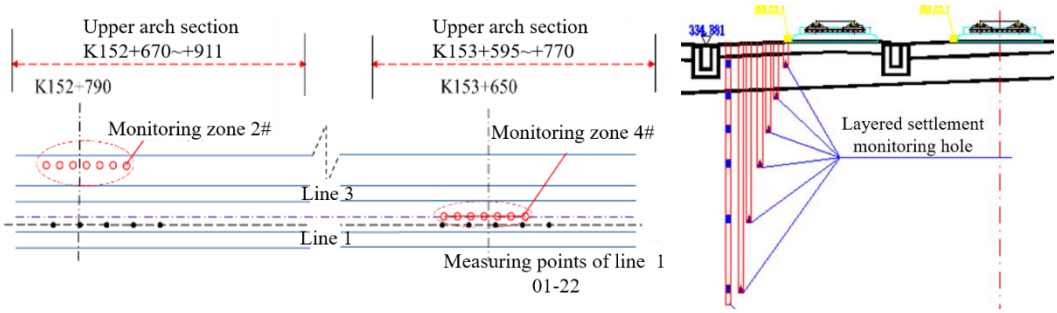

Figure 4: Monitoring points.

The depths of the monitoring holes for layered uplift deformation were set at 0.8m, 2.0m, 3.0m, 4.0m, 6.0m, 10m, 15m, and 20m. By calculating the deformation differences at different depths within the same array, layered uplift values for different depth intervals were obtained. The monitoring continued until the renovation of the embankment in 2020, with a duration of more than 5 years.

4.1 Surface Uplift Deformation

Table 2 presents the observed values of surface uplift for the 22 measurement points along Mainline I from June 2015 to June 2020, covering a period of 5 years. The range of values is between 7.77mm and 48.55mm, with most values exceeding the track deformation control limit. A comparison of the data in the table reveals significant differences in the uplift amounts at various points along the longitudinal axis of the track. Sudden changes are observed between some points, such as a variation from 12.83mm to 39.30mm in the uplift amount within a 20m distance between points 6 and 7, resulting in an uplift difference of 26.47mm and an angular deflection of 1.3‰. This has a substantial impact on the smooth operation of high-speed trains.

Measuring points of line 1	Upward displacement /mm	Measuring points of line 1	Upward displacement /mm
1#	7.77	12#	28.90
2#	12.45	13#	12.44
3#	15.54	14#	13.59
4#	22.06	15#	18.66
5#	14.67	16#	23.06
6#	12.83	17#	31.06
7#	39.30	18#	30.34
8#	48.55	19#	23.02
9#	38.66	20#	15.72
10#	29.65	21#	8.45
11#	28.90	22#	10.50

Table 2: Arch deformation of the roadbed surface.

Figure 5 illustrates the typical uplift time-history curve for the embankment surface at the 8# measurement point with the maximum uplift. From the graph, it can be observed that over the 5-year observation period, the embankment exhibits a sustained and gradual upward uplift deformation: 1) Although the uplift time-history curve shows some fluctuations, the overall trend indicates inconspicuous convergence; 2) The uplift rate is relatively small, with an average monthly uplift rate of only 0.81mm at the 8# measurement point with the maximum deformation. However, the cumulative uplift over 5 years has reached 48.55mm.

To analyze the annual variation in embankment uplift rates, the yearly average uplift rates were calculated at six-month intervals, with observations for the first half-year marked in March and those for the second half-year marked in September, as shown in Figure 6. From Figure 6(a), it can be observed that the uplift rate time-history curves for each measurement point exhibit a similar changing pattern. Specifically, from 2015 to 2016, the annual uplift rates were relatively high, and there was a rapid decrease in uplift rates. However, from 2017 to 2020, the annual uplift rates did not show a continuous decreasing trend but rather stabilized within a certain fluctuation range. As depicted in Figure 6(b), at measurement points 8# and 17#, which experienced significant uplift, the annual uplift rates gradually stabilized in the range of 5 to 11mm/year. This suggests that the embankment is uplift at a stable rate each year, and there is currently no apparent trend of convergence.

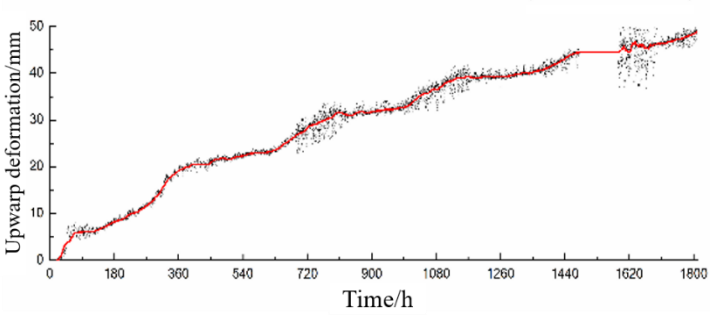

Figure 5: Typical time-history curve of arch deformation (8#).

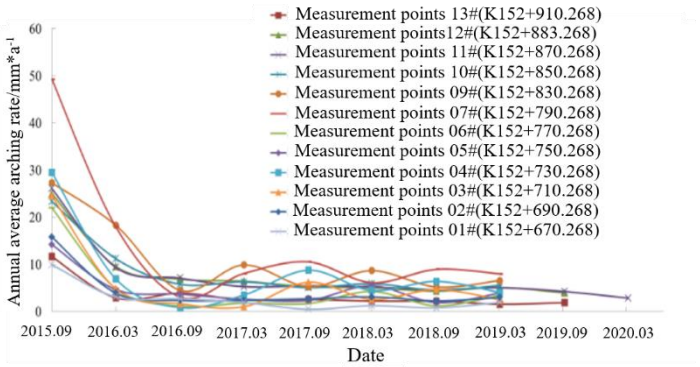

(a) Annual average uplift rate time-history curve

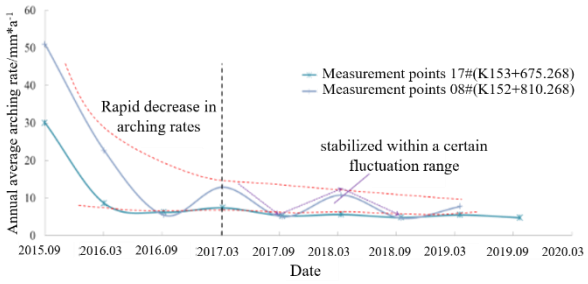

(b) Annual average uplift rate time-history curves for Points 08 and 17

Figure 6: Time-history curve of annual average arch rate.

At the same time, the time-history curves of embankment uplift rates exhibit obvious periodic fluctuation characteristics. The following analysis explores the correlation between these fluctuation features and the local rainfall cycles. For the Sichuan region, located in the subtropical humid climate zone of Central Asia, the annual precipitation shows significant seasonality, with June to September being the rainy season and November to April being the dry season. Corresponding to the local wet-dry season variations, the average embankment uplift rates from May to October and from November to April were calculated for representative measurement points

10# and 20#. The annual fluctuation patterns are illustrated in Figure 7. It can be observed from the figure that the peaks of the uplift rates occur in the rainy season, specifically in July and August, while the troughs, indicating the lowest uplift rates, are observed during the dry season in January and February. The fluctuation of embankment uplift rates aligns well with the periodic wet-dry season changes, indicating the significant influence of environmental rainfall variations on embankment uplift.

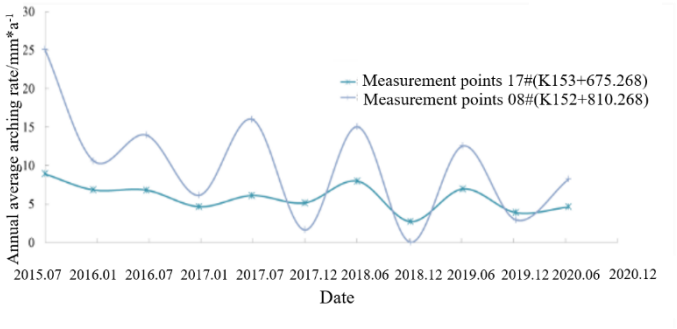

Figure 7: Periodic variation of uplift rate with rain dry season.

Figure 8 presents longitudinal distribution maps of uplift deformations at various stages for each measurement point along Line I.

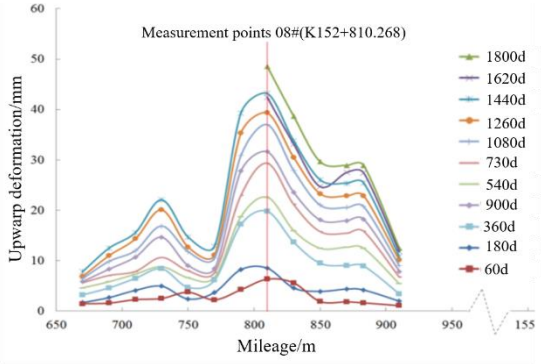

Figure 8: Vertical distribution of arch deformation.

The uplift deformations are spatially uneven, exhibiting multiple peaks such as at Points 3 and 8. Notably, there is a prominent peak at Point 8, indicating rapid development. Simultaneously, some points show lower uplift rates compared to the surrounding points, gradually forming concave points, as seen at Points 6 and 10. The longitudinal distribution of uplift deformations in the roadbed surface layer demonstrates an uneven pattern, and its development trend continues to evolve. When the "convex" points and "concave" points are in close proximity, such as at Points 6 to 8, significant differences in uplift quantities can occur, adversely affecting the smoothness of the track.

The reasons for this uneven uplift deformation could stem from various factors, including the non-uniform distribution of moisture-absorbing fissures and variations in the expansive potential of the underlying mudstone. All factors that could lead to

uneven deformation in the underlying bedrock would influence the development of uplift deformation in the roadbed surface layer.

4.2 The uplift deformation in the underlying layers

The spatial and temporal distribution characteristics of uplift deformation in the underlying layers of the embankment base are obtained through multiple single-point settlement gauges, each reflecting the relative deformation of rock layers within a specific depth range. The time-series curves of monitoring values for different depth layers from December 2017 to June 2020 are shown in Figure 9. It can be observed that the relative deformation values of different depth layers follow similar patterns over time: (1) The test values of single-point settlement gauges are all positive, indicating that the relative deformation of rock layers is in tension, confirming the presence of uplift deformation in the underlying layers of the embankment. (2) The relative uplift deformation values at different depths continue to increase over time. The changing trend is generally consistent, aligning with the characteristics of the previously discussed time-series curves for surface uplift. The growth rate shows some fluctuations but, overall, does not exhibit a clear convergence trend.

Comparing monitoring values at different depths reveals that with increasing depth, the observed relative uplift values of rock layers also increase. The incremental difference reflects the stratified uplift deformation from one depth to another. For example, in monitoring zone 2#, the observation value at the depth of 0.8m is 0.77mm, and at the depth of 3.0m, it is 3.18mm. The difference of 2.41mm represents the stratified uplift deformation within the depth range of 0.83.0m. Table 3 provides an analysis of the stratified uplift amounts at different depth intervals. From the table, it can be observed that, for monitoring zone 2#, the distribution of stratified uplift amounts along the depth is uneven. The most significant uplift occurs not in the shallowest part but in the rock layers between 610m, accounting for 67% of the total uplift amount. For monitoring zone 4#, the stratified uplift amounts are most significant in the 0.03.0m and 6.015.0m intervals, each accounting for over 40% of the total uplift amount. The stratified uplift amount in the 15~20m interval is minimal or even negative, indicating that the rock layers below 15m have not undergone significant uplift deformation.

Comprehensive monitoring results from two observation areas reveal that the depth of rock layers contributing to uplift deformation reaches 10-15m. Significant differences are observed in the stratified uplift deformation of rock layers across different depth intervals, with main uplift layers concentrated within specific depth ranges. These patterns likely stem from the non-uniform characteristics of the structure and composition of the red beds in the Sichuan Basin. Interlayer interfaces in the mudstone-sandstone structure and macroscopic fracture surfaces in the mudstone serve as primary channels for moisture migration[20]. Uneven distribution of these interfaces and surfaces along depth leads to considerable variation in stratified uplift deformation of rock layers. In essence, stratified uplift deformation in the red beds is primarily determined by the distribution of layer interfaces and fracture surfaces along the bedrock depth, differing from patterns observed in uniformly expansive soils and rocks influenced by atmospheric conditions.

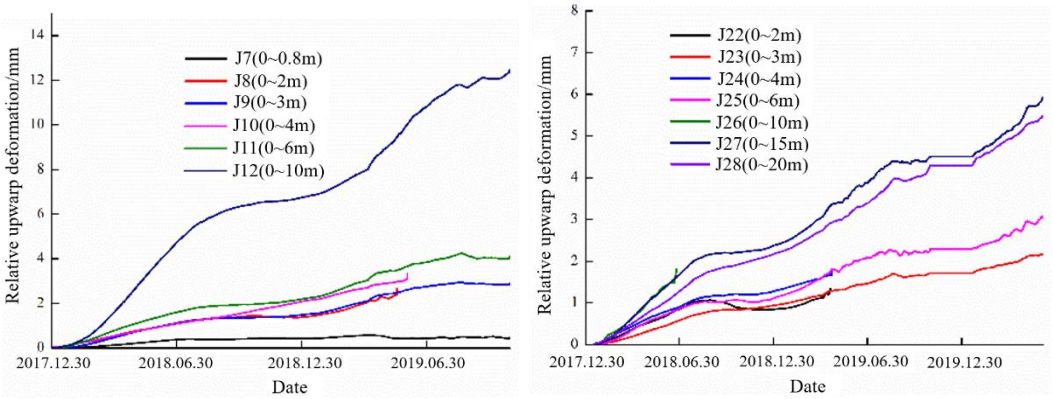

(a) : Monitoring zone 2#. (b) : Monitoring zone 4#.

Figure 9: Time-history curve of relative arch deformation at different depths.

Monitoring zone	Depth/m	Relative displacement /mm	Layered uplift displacement /mm	Layered uplift displacement / Maximum uplift displacement /%
2#	0.8	0.77	0.77	6%
	3.0	3.18	2.41	19%
	6.0	4.2	1.79	8%
	10.0	12.58	8.38	67%
4#	3.0	2.64	2.64	42%
	6.0	3.67	1.03	17%
	15.0	6.42	2.75	44%
	20.0	6.22	-0.2	-3%

Table 3: Analysis table of stratified uplift deformation in the bedrock layers.

Considering the pattern of uplift deformation in the roadbed surface, it is evident that this deformation is, in fact, the cumulative result of stratified uplift in the underlying bedrock. Therefore, the spatiotemporal characteristics of uplift deformation in the roadbed surface are influenced by factors such as the elevation of the main deformation layers in the underlying bedrock, burial depth, and the deformation development capacity. These factors collectively influence the macroscopic manifestation of uplift deformation in the roadbed.

5 The mechanism influencing the continuous uplift deformation in the roadbed

Integrating the above analyses, we discuss the mechanism underlying continuous uplift deformation in the roadbed due to the non-uniform characteristics of the geological structure, mineral composition, microstructure, and expansiveness in the Sichuan basin Red Bed formation.

Macroscopically, the Sichuan Red Beds predominantly comprise interlayered mudstone and sandy rocks with nearly horizontal bedding. These rock types exhibit significant differences in fissure development and expansiveness, with weakly weathered mudstone showing expansiveness over 2 MPa, two orders of magnitude higher than sandy rocks. Anisotropic analysis reveals the main expansion direction perpendicular to the bedding plane, causing joint fissure surfaces along these planes, facilitating water migration into deeper layers. Layered uplift data suggests a close relationship between primary deformation layers and the distribution of rock layers, bedding planes, and fissure surfaces. Mudstone's poor permeability leads to expansive deformation at interfaces and fissures, particularly dense bedding planes and fissure surfaces. The hydraulic connection interfaces can extend depths exceeding 15 meters, differing fundamentally from typical expansive soils controlled by atmospheric conditions.

Microscopically, the mineral composition of the Sichuan Red Beds, especially expansive clay minerals, exhibits significant non-uniformity. Curled clay minerals lining between platy fragments in pores and micro-cracks result in substantial internal expansive forces exceeding 1500 kPa, generating new micro-cracks and facilitating water infiltration along fracture surfaces.

In terms of spatiotemporal evolution, water migration is gradual, starting from the surface and penetrating deeper into the material. A humidity gradient field forms, leading to differential expansive potential release between fracture surfaces and the matrix interior. This non-uniform expansion manifests in both temporal evolution and spatial distribution, contributing to macroscopic fracture surface extension and interconnected microcrack generation, facilitating further water migration and triggering cycles of non-uniform expansive deformation. Influenced by long-term environmental changes, this cyclic process is a crucial mechanism for sustained micro-upward deformation in high-speed railway subgrades.

6 Conclusions

In conclusion, the Sichuan Red Beds region exhibits a distinctive rock structure characterized by alternating layers of mudstone and sandstone, presenting variations in strength, permeability, and the non-uniform distribution of macroscopic joint and fracture surfaces. The mineral composition of these beds contains significant amounts of expansive clay minerals, with notable differences in types and content. Microscopically, the curled clay minerals within the Sichuan Red Beds, surrounding plate-like fragmented particles in pores and fractures, determine its anisotropic expansivity. The vertical expansion rate ranges from 2.73% to 5.83%, with anisotropic expansion rates indicating significant differences. Expansion forces vary widely, ranging from 449.9 kPa to 2025.5 kPa, showing highly non-uniform characteristics. The subgrade's initial upward deformation rate decreases rapidly after the first 1-2 years of operation, stabilizing within a fluctuation range of approximately 5-11 mm annually thereafter. This upward deformation, extending to depths of 15 meters or more, is primarily controlled by the distribution of rock layer fractures. The ongoing evolution of non-uniform expansion and fracturing, influenced by environmental cyclic changes, leads to long-term upward deformation of the subgrade at a relatively

low rate. Consequently, careful consideration of these factors is essential when constructing deformation-sensitive structures such as high-speed railways in the Sichuan Red Beds region.

Acknowledgements

This research was funded by the National Natural Science Foundation of China (No. 42172308), the Youth Innovation Promotion Association CAS (No. 2022331).

References

[1] M. Ji, F. Gao, Y.N. Gao, et al. "Study on time-dependent effect of calcareous mudstone expansion after infiltrated with water", Journal of China University of Ming and Technology, 39(4), 511-515, 2010.

[2] X.L. Liu, S.J. Wang, E.Z. Wang, et al. "Study on time-dependent swelling constitute relation of swelling rock". Journal of Hydraulic Engineering, 37(2), 195-199, 2006.

[3] K. Huang, Z.J. Dai, C.Z Yan, et al. "Swelling behaviors of heterogeneous red-bed mudstone subjected to different vertical stresses", Journal of Rock Mechanics and Geotechnical Engineering, 1674-7755, 2024.

[4] R. Doostmohammadi, M. Moosavi, T. Mutschler, et al. "Influence of cyclic wetting and drying on swelling behavior of mudstone in south west of Iran", Environmental Geology, 58(5), 999-1009, 2009.

[5] Z. Zhou, S.X. Chen, Z.J. Dai, et al. "Study on the strength softening law of Cenozoic red sandstone based on point load test". Geotechnical mechanics, 42 (11), 2997-3007, 2021.

[6] Z.J. Dai, J.H. Guo, F. Yu, et al. "Long-term uplift of high-speed railway subgrade caused by swelling effect of red-bed mudstone: case study in Southwest China". Bulletin of Engineering Geology and the Environment, 80(6), 4855-4869, 2021.

[7] Z.B. Zhong, A.H. Li, R.G. Deng, et al. "Study on time-dependent upheaval deformation mechanisms of red-bed soft rock subgrade of high-speed railways", Chinese Journal of Rock Mechanics and Engineering, 39(02), 327-340, 2020.

[8] F. Yu, K.W. Tong, Z.J. Dai, et al. "Macro- and micro research on swelling characteristics and deformation mechanism of red-bed mudstone in central Sichuan, China". Geofluids, 2022, 1-18, 2022.

[9] G.S. Feng, F. Yu, Z.J. Dai, et al. "Experimental study on time effect characteristics of red mudstone swelling in Central Sichuan", Chinese Journal of Rock Mechanics and Engineering, 41(S1), 2780-2790, 2022.

[10] K. Huang, F. Yu, Z. Zhou, et al. "Influence of pH on moisture-absorbing swelling cracks of red layer in central Sichuan and its micro-mechanism", Environmental Earth Sciences, 81, 441, 2022.

[11] P.P. Wu, "Numerical analysis on the long-term upheaval deformation of high-speed railway deep cutting based on rheology", Subgrade Engineering, (1), 135-139, 2019.

[12] Y. Ji, Q.G. Liang, J.Y. Guo, et al. "Study on deformation law of deep foundation of high-speed railway in red layer soft rock area", Journal of Railway Science and Engineering, 18(3), 572-580, 2021.
[13] T.Y. Zhang, L.N. Ma, R.L. Zhang, et al. "Experimental study on swelling characteristic of mudstone foundation of high-speed railway", Journal of Railway Science and Engineering, 16(04), 871-877, 2019.
[14] B.Z. Wang, Q.C. Wang, R.L. Zhang, et al. "Attenuation law of expansion deformation rate and water migration rate on mudstone of ballastless track foundation", Hydro-Science and Engineering, (2), 41-47, 2019.
[15] Z.J. Dai, J.H. Guo, F. Yu, et al. "Long-term uplift of high-speed railway subgrade caused by swelling effect of red-bed mudstone: case study in Southwest China". Bulletin of Engineering Geology and the Environment, 80(1), 2021.
[16] S.X. Chen; Z. Zhou; F. Yu, et al. "Study of evolution law of cracking for swelling mudstone of Sichuan central Redbeds in hydration process", Japanese Geotechnical Society Special Publication, 7(2), 96-101, 2019.
[17] H.W. Jing, "Water-physical property of Sichuan central red-beds and its influence on the deformation mechanism analysis ballastless track", Journal of Geological Hazards and Environment Preservation, 30(02), 35-40, 2019.
[18] S. Zhang, Q. Xu, Z.M. Hu, "Effects of rainwater softening on red mudstone of deep-seated landslide, Southwest China", Engineering Geology, 204, 1-13, 2016.
[19] C.Y. Zhou, D.L. Su, X.L. Qiu, et al. "Experimental study of cracked soft rock with hydro-mechanical coupling effect", Acta Scientiarum Naturalium Universitatis Sunyatseni, 58(6), 35-44, 2019.
[20] K. Huang, F. Yu, W. Zhang, et al. "Relationship between capillary water absorption mechanism and pore structure and microfracture of red-layer mudstone in central Sichuan", Bull Eng Geol Environ, 82, 100, 2023.